Available online at www.sciencedirect.com
ScienceDirect
Thermochimica Acta 454 (2007) 69–77
thermochimica acta
www.elsevier.com/locate/tca

# Reduction kinetics of mechanically activated hematite concentrate with hydrogen gas using nonisothermal methods

Parviz Pourghahramani *, Eric Forssberg

*Division of Mineral Processing, Luleå University of Technology, SE-971 87 Luleå, Sweden*

Received 10 August 2006; received in revised form 22 December 2006; accepted 22 December 2006
Available online 9 January 2007

**Abstract**

The reduction kinetics of both non-activated and mechanically activated hematite concentrate in a vibratory mill for different grinding periods have been studied using themogravimetry (TG). Changes in the structure of hematite were studied using X-ray diffraction analysis. The isoconversional method of Kissinger–Akahira–Sunose (KAS) was used to determine the activation energy of the different reactions. The Vyazovkin model-free kinetic method was also used for prediction of kinetic behavior of the samples for a given temperature.

$Fe_2O_3$ was found to reduce to Fe in a two-step via $Fe_3O_4$. Intensive grinding resulted in improved resolution of overlapping reduction events. It was also established that the mechanical activation had a positive effect on the first step of reduction. With increasing the grinding time, the activation energy at lower extent of conversion ($\alpha \leq 0.11$) decreased from 166 to 106 kJ mol$^{-1}$ range in the initial sample to about 102–70 kJ mol$^{-1}$ in the sample ground for 9 h. The complexity of the reduction of hematite to magnetite and magnetite to iron was illustrated by the dependence of $E$ on the extent of conversion, $\alpha(0.02 \leq \alpha \leq 0.95)$. The values of $E$ decreased sharply with $\alpha$ for $0.02 \leq \alpha \leq 0.11$ range in the initial sample and mechanically activated samples, followed by a slight decrease in the values of $E$ during further reduction by $\alpha \leq 0.85$ in the ground samples up to 3 h. A slight increasing dependence of $E$ on $\alpha$ for mechanically activated sample within 9 h in the second step of reduction was observed due to the finely agglomerated particles during intensive milling and subsequently the formation of a dense layer during the reduction processes. In addition, the dependence of $\ln A_\alpha$ on $\alpha$ was detected and it was found that the $\ln A_\alpha$ shows the same dependence on $\alpha$ as the apparent activation energies.


*Keywords:* Mechanical activation; Iron oxide; Reduction kinetics; Themogravimetry; Nonisothermal

## 1. Introduction

The reduction of iron oxides by hydrogen has been investigated extensively because of its relevance to iron production. The existence of a series of three successive reactions from hematite ($Fe_2O_3$) to iron through magnetite and wüstite ($Fe_{1-x}O$) is of interest from an academic point of view, regarding the possibility of coupling between two steps and the consequences of each step upon the following one. The literature [1,2] suggests that the reduction of $Fe_2O_3$ to iron metal, at lower temperature below 570 °C, proceeds in two steps via $Fe_3O_4$ intermediate as follows:

$$3Fe_2O_3 + H_2 \rightarrow 2Fe_3O_4 + H_2O \qquad \text{step1} \qquad (1)$$

$$Fe_3O_4 + 4H_2 \rightarrow 3Fe + 4H_2O \qquad \text{step2} \qquad (2)$$

Step 1 is exothermic, whilst reduction to the metal in step 2 is endothermic [2]. Excellent agreements were achieved in the rate-controlling reactions. Kinetics data for the reduction of iron oxides are generally described in terms of nucleation/autocatalytic, diffusion and phase boundary models. However, discrepancies exist among the reported kinetics models for the reduction steps. Such inconsistencies may be attributed to the starting raw material characteristics, sample specimen used (powder, pellet, or ore), nature of reducing gas, temperature range, reduction step, presence of water, gas impurities, physical shape, etc. [3,4]. It is generally agreed that the rate of reduction by $H_2$ is significantly faster than that by CO [5]. However, during the final stage of reduction, the rate with hydrogen decreases compared with CO. In the reduction of iron ores with hydrogen, a dense iron shell forms around the particles (magnetite and/or wüstite grains) and subsequently inhibits gaseous transport during reaction [1,6,7]. Several investigations have been reported

* Corresponding author. Tel.: +46 920 491313; fax: +46 92097364.
*E-mail address:* Parviz.Pourghahramani@ltu.se (P. Pourghahramani).

0040-6031/$ – see front matter © 2007 Elsevier B.V. All rights reserved.
doi:10.1016/j.tca.2006.12.023

that the reduction of $Fe_2O_3$ is catalyzed by metal additives in the presence of water vapor (2–7.5%, v/v in reducing mixture). This enhancement is ascribed to "hydrogen spill over" effect which provides the necessary active hydrogen at the reduction centers [2,8]. However, the addition of $H_2O$ retards generally the reduction rate, especially for $Fe_3O_4 \rightarrow Fe$ step [3].

The concept of high-energy milling has attracted considerable scientific and technical interests in recent years as a consequence of higher reactivity and properties developed by this process. Mechanical activation has found a wide range of application potential such as the intensification of thermal reactivity of minerals [9]. Mechanical activation has usually a positive influence on the leaching reaction kinetics. In addition, the mechanical activation of minerals makes it possible to reduce their reaction temperature and/or their decomposition temperature or causes such a degree of disordering. Thermal behavior of mechanically activated galena and pyrite has been investigated by Hu et al. [10–12]. It has been found that mechanically activated pyrite and galena are more easily decomposed during thermal treatments than non-activated pyrite and galena. Moreover, the activation energy of the thermal decomposition of pyrite decreases as a consequence of mechanical activation. Mechanically activated sphalerite also oxidizes easily than non-activated sphalerite [13]. Milling of manganese ore with graphite led to enhanced reduction at decreased temperatures [14]. Mechanical activation of hematite concentrate can result in reduction of hematite to maghemite ($\gamma$-$Fe_2O_3$), magnetite and subsequently to FeO [15,16]. Since oxygen bonds on the hematite surface are broken, oxygen is released during high energy milling of hematite particles in air. However, the transformation of all hematite by milling process occurs after relatively long period of time. It is thought that the mechanical activation with a low temperature heat treatment can be successfully applied for reduction of hematite to magnetite.

The goal of this paper is to study the reduction kinetics of both non-activated hematite and mechanically activated hematite in a vibratory mill for various grinding times.

## 2. Experimental

### 2.1. Material

The high-purity hematite concentrate used in this study was kindly supplied by the LKAB (Luossavaara Kiirunavaara Aktiebolag) company in Sweden. The chemical analysis showed that the initial hematite powder contained about 97.91% $Fe_2O_3$, 0.73% $Al_2O_3$, 0.73% $SiO_2$, 0.26% $TiO_2$, 0.20% MgO, 0.022% MnO, and 0.088% $P_2O_5$. Other components such as $K_2O$, CaO and $Na_2O$ comprise 0.051%. The X-ray diffraction analysis represented only the hematite diffraction peaks.

### 2.2. Mechanical activation

The dry grinding tests were carried out using a vibratory ball mill with dimensions of *L*320 mm × Ø185 mm. A mixture of ball steel media with dimensions between 6 and 22.2 mm and with apparent density of 4875 kg m$^{-3}$ was used as grinding media.

Table 1
Milling conditions in the vibratory mill

| Milling conditions | Vibratory milling |
|---|---|
| Media filling (%) | 70 |
| Mass of media (kg) | 33.16 |
| Milling time (h) | 1, 3, 9 |
| Ball to powder weight ratio | 67.68:1 |
| Speed (RPM) | 1000 |
| Amplitude (mm) | 8 |

Milling experiments were made in air atmosphere under closed milling condition, i.e., the door of mill was kept closed during the whole milling process periods. The grinding conditions are summarized in Table 1. The samples were sealed into plastic tubes and kept in a freezer for further measurements.

### 2.3. Characterization

Thermogravimetric analyses (TG) were conducted with a NETZSCH STA 409C instrument at three heating rates of 10, 15 and 20 °C min$^{-1}$ from room temperature to 850 °C. The high temperature furnace was heated by graphite heating elements, which were protected by injection of inert argon gas. The temperature of furnace was controlled by a tungsten thermocouple. The heating was performed under highly pure hydrogen as reduction gas with a flow rate of 100 ml min$^{-1}$. The mass of samples was almost 95 mg.

The morphological characterization of the samples was performed using a Philips XL 30 scanning electron microscope (SEM) equipped with a $LaB_6$ emission source and running at 20 kV. After drying, the samples were gold coated using gold sputtering prior to SEM investigation.

The XRD patterns were obtained using a Siemens D5000 powder diffractometer with Bragg-Brentano geometry equipped with a curved graphite monochromator in the diffracted beam arm and using Cu Kα radiation ($\lambda = 0.15406$ nm). The XRD patterns of the samples were recorded using a step size of 0.02° and a counting time of 5 s per step.

## 3. Kinetic analysis

Several methods have been applied for kinetics studies of solid state reactions [17]. The methods of kinetics analysis can be classified based on experimental conditions selected and the mathematical analysis performed. The mathematical methods are divided into model fitting and isoconversional (model-free) methods. Modelistic methods have been criticized in nonisothermal studies because (1) they assume a constant kinetic triplet (*A*, *E* and model), (2) they involve fitting three parameters (*A*, *E* and model), which are simultaneously determined from a single curve, (3) they involve a single heating rate, which is not always sufficient to determine reaction kinetics and (4) the selection of the best model is a challenging task based on a statistical parameter ($r^2$) [18–22]. Model fitting methods were the most popular methods in the analysis of solid state kinetics. The popularities of these models have recently declined in favor of isoconversional methods which can compute kinetics parameters without

modelistic assumptions [22,23]. On the other hand, a successful kinetics analysis can be performed using several experiments at the same degree of conversion if careful experiments will be applied considering the suggestions by Ortega [24]. The basic assumption of isoconversional methods is that the reaction rate at a constant conversion is only a function of temperature, and the reaction model is independent of temperature of heating rate [25–28]. Thus, constant $E$ values may be expected in the case of single-state decomposition, while a multi-step reaction $E$ varies with conversion degree due to the variation in the relative contributions of the single step to the overall reaction rates. The goal of the model-free kinetics analysis is to use this variation, as an additional source of information on the reaction mechanism [29,30]. The main disadvantage of isoconversional approach is that they do not suggest direct evaluation of the pre-exponential factor without kinetic model. To use the isoconversional methods, a series of experiments has to be conducted at different heating rates [31].

In the kinetic analysis, a reaction progress expresses conventionally in terms of conversion fraction or extent of reaction as:

$$\alpha = \frac{w_i - w}{w_i - w_f} \tag{3}$$

where $w_i$, $w$ and $w_f$ are the initial, actual and final weight of the sample, respectively.

The rate of a solid state reaction can be described by:

$$\frac{d\alpha}{dt} = \beta\frac{d\alpha}{dT} = k(T)f(\alpha) = A\exp\left(\frac{-E}{RT}\right)f(\alpha) \tag{4}$$

where $k(T)$ is the rate constant at temperature $T$, $f(\alpha)$ is a function of $\alpha$ which represents the reaction mechanism, $\alpha$ the extent of reaction, $t$ is the time and $\beta$ is the heating rate. $A$ and $E$ correspond to the pre-exponential and activation energy, respectively. Eq. (4), can be expressed in the form of its integral, $g(\alpha)$, with Eq. (5).

$$g(\alpha) = \int_0^\alpha \frac{d(\alpha)}{f(\alpha)} = \frac{A}{\beta}\int_0^T \exp\left(\frac{-E}{RT}\right)dT;$$

$$\text{If } \frac{E}{RT} = x \Rightarrow g(\alpha) = \frac{AE}{\beta R}\int_x^\infty \frac{e^{-x}}{x^2}dx = \frac{AE}{\beta R}\int_x^\infty p(x)dx \tag{5}$$

where $p(x)$ is the temperature integral. The Eqs. (4) and (5) underlie most of the methods of kinetics processing. Several reaction models used in the analysis of solid state kinetics are listed in Appendix A in terms of $g(\alpha)$ and $f(\alpha)$. The $p(x)$ has no analytic solution, but several approximations have been made. One of the most widely used approximations has been given by Coats and Redfern [32,33] for exponential $p(x)$:

$$\ln\frac{g(\alpha)}{T^2} = \ln\left(\frac{AR}{\beta E}\left[1 - \left(\frac{2RT_{exp}}{E}\right)\right]\right) - \frac{E}{RT}$$

$$\text{If}: \left(\frac{2RT}{E}\right) \ll 1 \Rightarrow \ln\frac{g(a)}{T^2} = \ln\left(\frac{AR}{\beta E}\right) - \frac{E}{RT} \tag{6}$$

where $T_{exp}$ is the mean experimental temperature. A plot of $\ln g(\alpha)/T^2$ versus $1/T$ gives activation energy and pre-exponential factor from the slope and intercept of the curve with a single heating rate, respectively. All integral functions in Appendix A can be tested and the best method can be selected with regard to a statistical parameter such as correlation coefficient ($r$).

On the other hand, the isoconversional methods calculate the kinetics parameters at a progressive degree of conversion ($\alpha$) without the modelistic assumptions. Among the isoconversional methods, Kissinger–Akahira–Sunose (KAS) [34,35] method has been widely used to estimate activation energy regardless of the rate expressions of reactions as follows:

$$\ln\frac{\beta}{T^2} = \ln\left(\frac{AE}{g(\alpha)R}\right) - \frac{E}{RT} \tag{7}$$

For $\alpha$ = const., the plot $\ln \beta/T^2$ versus $1/T$ obtained from curves recorded at several heating rates, should be a straight line whose slope can be used to calculate the activation energy. In the present paper, the above mentioned methods were used for calculation of the kinetic parameters of the reduction of mechanically activated and non-activated hematite samples to iron.

The isoconversional method provides a model-free way of making kinetic predictions. Furthermore, model-free kinetics does not need the experimental values of $A$, and $g(a)$ or $f(a)$ for the practical purposes of kinetic predictions. The respective predictive equation [37,38] was given in the following form assuming the partial kinetic triplets remain the same over the temperature region related to a given conversion:

$$t_\alpha = \frac{\int_0^{T_\alpha}\exp(-E_\alpha/RT)dT}{\beta\exp(-E_\alpha/RT_0)} \tag{8}$$

This enables the time, $t_\alpha$, at which a given conversion will be reached at an arbitrary temperature, $T_0$, to be computed. $T_\alpha$ is an experimental value of the temperature corresponding to a given conversion at the heating rate $\beta$ and $E_\alpha$ is the activation energy at a given conversion.

## 4. Results and discussion

### 4.1. X-ray diffraction analysis

The XRD patterns of non-activated and activated samples are given in Fig. 1. Considering the peaks of non-activated and activated hematite, the X-ray patterns of the milled samples only show the Bragg reflections of hematite, suggesting that the starting material did not undergo significant reactions either during milling or after prolonged milling. With the increased grinding time, a continuous broadening of the diffraction peaks and decreased intensity of diffraction peaks were observed. These indicate an increase in the degree of lattice disorder and a decrease in the crystallite size, thereby reducing the symmetry of the unit cell until some fraction of the material becomes amorphous. Comparing the XRD patterns indicates that the maximum line broadening and minimum intensity are obtained for hematite sample ground for longer time. In literature [9,11], it was reported that the mechanical activation resulted in the amorphization of minerals, development of large numbers of dislocation and their associated strain fields, decrease of crys-

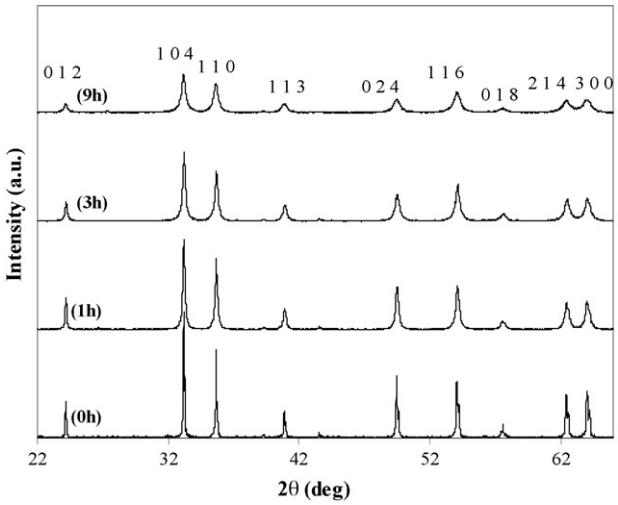


Fig. 1. X-ray diffraction patterns of non-activated and activated hematite. Hereafter, 0 h refers to the initial sample or non-activated sample.

tallite size and change of the lattice parameters which might lead to an overall decrease in long range lattice periodicity. This may be interpreted as the formation of a metastable "amorphous phase", because line broadening and the reduction of diffraction peaks intensity take place on X-ray pattern after prolonged milling.

### 4.2. Reduction behavior

Conventionally, reduction kinetics of iron oxides, such as hematite or magnetite, has been studied in terms of the extent of reaction ($\alpha$). Fig. 2 shows changes in the degree of conversion with three different heating rates for the reduction of the initial sample by $H_2$ as a function of temperature. A close look on the curves indicates slight changes of slopes at different temperatures, the changes are more prominent at lower and higher temperature ranges. These are indicative of sequential reactions. The changes in the slope of the curves at $\alpha = 0.11$ correspond to the quantitative conversion of hematite to magnetite. The production of 89% $H_2O$ associated with the subsequent reduction to Fe. The investigation of onset temperatures from the TG curves confirmed that the prereduction step to $Fe_3O_4$ is complete prior to the onset of the main reduction step to metal iron. This view is also supported by X-ray analysis of the reduction products

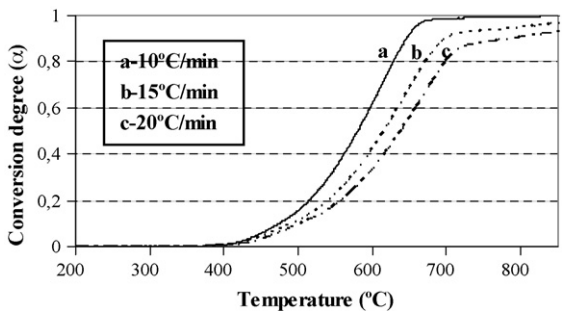


Fig. 2. Changes in the degree of conversion with three heating rates during the reduction of the initial sample as a function of temperature.

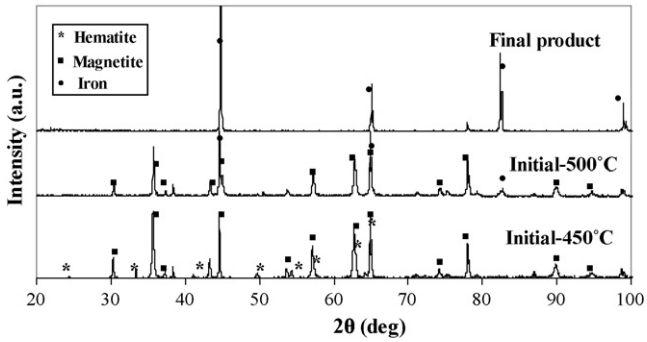


Fig. 3. XRD patterns of the reduction products of the initial sample. The products obtained under heating rate of 10 °C/min.

(Fig. 3). The XRD pattern of the reduction product of the initial sample heated to 450 °C with heating rate of 10 °C $min^{-1}$ represents both magnetite and hematite phases. The weight loss was calculated at about 2.87% up to 450 °C, which is still lower than the weight loss value corresponding to the complete conversion of hematite to magnetite (3.33%). The reduction of the initial hematite to 500 °C produces reflection peaks of magnetite and iron phases in the XRD powder pattern. As a result, the reduction proceeds stepwise ($Fe_2O_3 \rightarrow Fe_3O_4 \rightarrow Fe$). This agrees with previous literature studies on powder $Fe_2O_3$ sample which generally report that the reduction proceeds in two consecutive steps [1,2]. Sastri et al. [2] reported that the findings from X-ray diffractometry, Mössbauer spectroscopy and photomicrography studies showed that the reduction precedes in a stepwise manner with only two phases, either $Fe_2O_3$ and $Fe_3O_4$ or $Fe_3O_4$ and Fe, existing at any stages throughout isothermal reduction below 570 °C. It should be noted that the absence of wüstite in the XRD patterns of the reduction product does not mean that wüstite does not exist during the reduction because the dismutation reaction Fe $_{(1-x)}$ O can give Fe and magnetite.

According to Fig. 4, the slope of the curves corresponding to the activated samples changes when reaction progress reaches around 0.11. This indicates that the two steps of the reaction are resolved well as a result of mechanical activation. For non-activated hematite, the use of higher heating rates do not allow the complete conversion of hematite to iron metal at the same temperature ranges as it occurs for the samples ground by the mill. The maximum degree of conversion for all mechanically

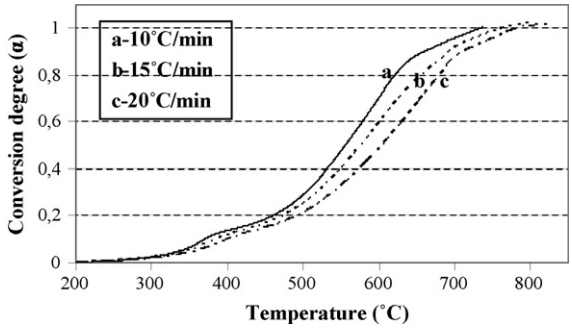


Fig. 4. Changes in the degree of conversion with three heating rates during the reduction of the sample ground for 9 h in the mill as a function of temperature.

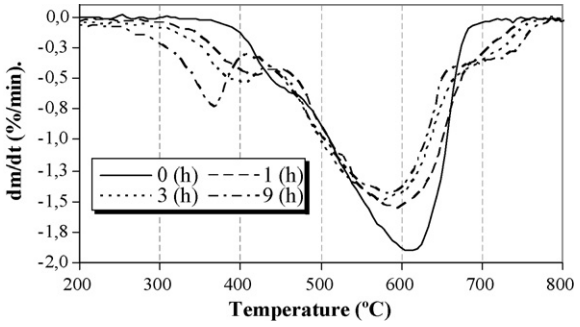


Fig. 5. TG curves of the initial sample and the samples ground for various grinding periods by the mill as a function of temperature.

activated samples is calculated close to unity, corresponding to the complete conversion of hematite to magnetite. It is clear that the reduction in the activated samples starts notably at lower temperatures (higher reactivity) than that in the initial sample. The beginning temperature of reaction decreases from 400 °C in the initial sample to about 250 °C in the sample ground for 9 h. Many workers have reported higher reaction rate at temperatures just below 600 °C than higher temperatures. Several reasons have been proposed for the occurrence of rate minimum [6,7]. These include sintering of the iron product which reduces diffusion of the reductant and the product gas to form the reaction interface. The rate minimum phenomenon is clear in the curve as shown in Fig. 4 at higher temperature for mechanically activated hematite.

The DTG curves corresponding to the heating rate of 10 °C $min^{-1}$ for the initial sample and the samples ground for different periods are shown in Fig. 5 as a function of temperature. The TG curves also represent a two-step weight loss which can be easily identified from the changes in the slope and the peaks of the curves. The first step of weight loss, corresponding to the reduction of hematite to magnetite, occurs at the lower temperatures. The second step (main step) of weight loss, the reduction of magnetite to iron, extends toward higher temperature sides up to 780 °C. Interestingly, the first step of weight loss is more pronounced for mechanically activated samples compared with the initial sample. In addition, a plateau between the two steps of reduction process can be observed. It is apparent that the resolution of the two events is greater for mechanically activated samples than for the initial sample. This is a consequence of the reduction of the energy required to reorganize the crystalline structure of hematite. The energy supplied by milling causes structural disorder through the distortion or breakage of the crystalline network. This was evident from the reduction of the intensities of XRD peaks reported in Fig. 1. Once more, this emphasizes that the mechanical activation results in improved resolution of overlapping reduction events. Moreover, the area of peak in the second step of reduction decreases concomitantly as the area of peak in the first weight loss step centered approximately between 300 and 450 °C increases, depending upon grinding time. For the non-activated hematite, the first step of reduction initiates and terminates at a certain temperature range. This is an expected property for crystalline hematite. However, activated hematite exhibits different starting and finishing temperatures of reduction in the first step of reduction, depending on grinding times and consequently the structural changes induced during milling.

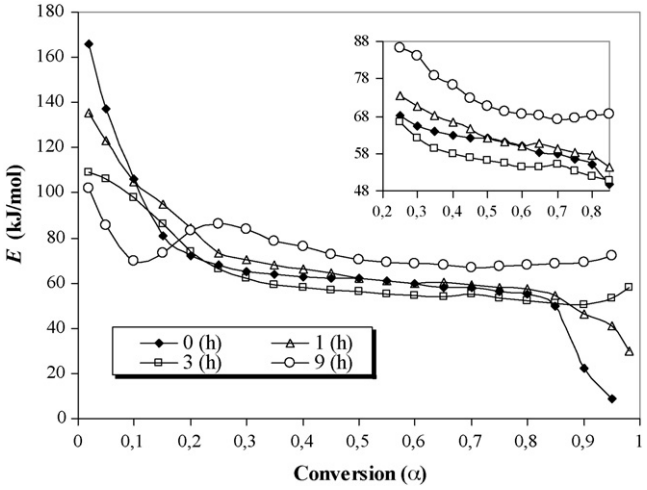


Fig. 6. Dependence of $E$ on $\alpha$ characteristic of the reduction of non-activated hematite and mechanically activated hematite for various grinding times; a large scale of the curves for the range of $0.25 \leq \alpha \leq 0.85$ are shown in inset.

### 4.3. Kinetic results

The application of the isoconversional methods requires the determination of the absolute temperature at which a fixed extent of reduction from the several TG curves recorded at different heating rates. The degree of conversion between 0.02 and 0.95 is investigated. The basic parameters such as conversion degree, heating rate and temperature were inserted into Eq. (7). The correlation coefficients for the linear regressions were higher than 0.94. The dependence of the activation energy $E$ on $\alpha$ characteristic for hydrogen reduction of non-activated hematite and mechanically activated hematite for different periods is shown in Fig. 6.

The overall decreasing dependence of the activation energy on $\alpha$ indicates that the overall reaction contains at least two steps. A decrease in the activation energy is most likely caused by transition of the limiting step from the higher activation energy reaction to the lower activation energy reaction. The curves corresponding to the initial sample and the mechanically activated samples show that $E$ decreases with extent of conversion ($\alpha$) by $\alpha \leq 0.11$, corresponding the reduction of hematite to magnetite, with increasing the grinding time. After this range, the activation energy continues to decrease for the initial sample and mechanically activated samples up to 3 h as opposed with the activation energy for mechanically activated sample within 9 h in which the activation energy tends to increase slightly and then decreases by $\alpha \leq 0.85$. The activation energy of the initial sample and ground sample for 1 h decrease drastically when the conversion degree exceeds 0.85 as opposed with the reduction of the activated samples for more than 1 h. Since the reduction of the initial sample and activated sample for 1 h extends up to 900 °C at higher heating rates, the decreases of the activation energy can probably be due to the phase transition of $\alpha$-Fe to $\gamma$-Fe (906 °C) [36].

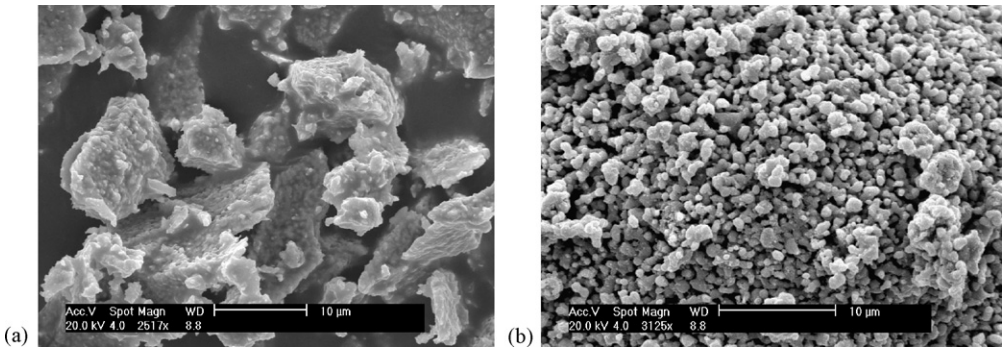


Fig. 7. SEM micrographs of the reduction products of the initial sample (a) and the sample ground for 9 h (b).

In the lower degree of conversion (lower temperature region), the reduction of non-activated hematite is much more sensitive to the extent of reaction. The first step of reduction, corresponding to $\alpha \leq 0.11$, in the initial sample describes with activation energy of about 166–106 kJ mol$^{-1}$, while the calculated value for the second reduction step, corresponding to $0.11 \leq \alpha \leq 0.95$, is about 72–9 kJ mol$^{-1}$. Comparison with literature data shows that discrepancies exist among the measured activation energies for the reduction of powdered iron oxides. Such variations may be associated with differences between the samples studied and or the conditions employed for sample reduction. For example, Munteanu et al. [39] reported the activation energies of 162 and 104 kJ mol$^{-1}$ for the first and second steps of the reduction using temperature-programmed method between 450 and 700 °C, where the precursor of $Fe_2O_3$ was ferrihydrite. Sastri et al. [2] reported that pretreatment at 850 °C of $\alpha$-$Fe_2O_3$ resulted in an increase in activation energy to 73 kJ mol$^{-1}$ relative to a value of 57 kJ mol$^{-1}$ for a sample that had undergone no heat treatment. Thus, the activation energy is strongly sample dependent and conditions employed for the reduction. The decreasing trend of activation energy in the two steps of the reduction can be explained in the terms of a nucleation and growth the model of reduction in which the activation energy required during nucleation is higher than that needed in the growth stage (autocatalytic effects). Similar trends have been reported for the reduction of iron oxides where $E$ has been found to decrease with extent of reduction using CR-TPR "rate Jump" technique [40].

For activated hematite, the activation energy for the range of $\alpha \leq 0.11$ decreases with increasing grinding time. The activation energy from 166 to 106 kJ mol$^{-1}$ range in the initial sample decreases to about 102–70 kJ mol$^{-1}$ in the sample ground for 9 h. The disordering of structure in mechanically activated samples brings about an increase in the rate of reduction process and a decrease in the activation energy [9]. For the second step of reduction, the ground sample up to 1 h exhibits no significant difference in activation energy by conversion degree of 0.85. Grinding for 3 h result in a slightly smaller activation energy compared with the initial sample; while prolonged milling for 9 h leads to higher activation energy than the initial sample. This can be attributed to the agglomeration of finely ground particles during intensive milling and subsequently to the formation of a dense layer as a result of the partial sintering at higher temperatures. As a result, the effect of disordering of hematite structure overlapped by the formation of the dense layer. Therefore, the reduction is retarded [5]. It can be concluded that mechanical activation has a positive effect on the prereduction step in terms of activation energy and small positive effect on the second step of reduction in the samples ground up to 3 h.

Furthermore, the dependence of the apparent activation energy ($E$) on the extent of conversion ($\alpha$) is a source of additional kinetic information of process [41]. The obtained results reveal that the dependence of the apparent activation energy ($E$) on the extent of conversion ($\alpha$) helps not only to disclose the complexity of reduction processes, but also to identify its kinetic scheme. A decreasing dependence of $E$ on $\alpha$ is often encountered in solid decompositions which follow: solid → solid + gas [38]. The curves obtained for non-activated sample and mechanically activated samples up to 3 h reveal a typical reversible reaction according to Vyazovkin et al. [38,42–44]. Vyazovkin and Linert [42] have been shown that the decreasing dependence of $E$

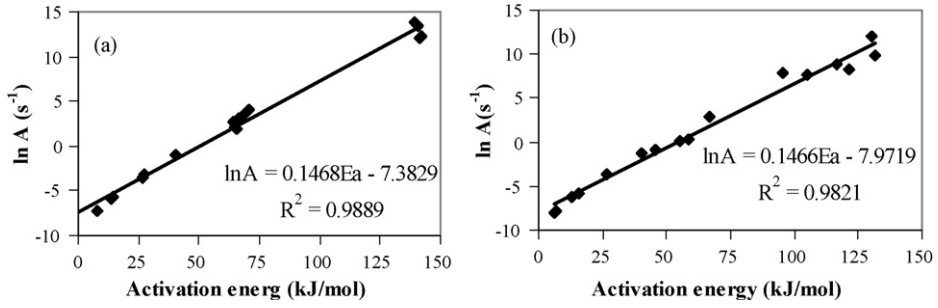


Fig. 8. The artificial isokinetic relationship (ln $A$ vs. $E$) using Coats–Redfern method at heating rate of 10 °C/min for the initial sample in the range of $0.02 \leq \alpha \leq 0.1$ (a), and $0.1 < \alpha < 0.95$ (b).

on $\alpha$ corresponds to the kinetic scheme of a reversible reaction followed by an irreversible one. For such process $E$ is limited by the sum of the activation energy of the irreversible reaction and the enthalpy of the reversible reaction at low conversions. At high values of conversions, $E$ is limited only by the activation energy of the irreversible reaction at high $\alpha$ [41]. In our case, the reduction of hematite to magnetite probably proceeds through the exothermic stage at low conversion degrees, which is characterized by a high value of the apparent activation energy between 166 and 70 kJ mol$^{-1}$ depending on the sample. The high values of the effective activation energy represent the sum of the enthalpy of the reversible process and of the apparent activation of the irreversible process. On the other hand, lower value of the activation energy at higher conversions is a characteristic of the process proceeding through a reversible endothermic process. For mechanically activated sample for 9 h, the decreasing dependence of the activation energy is followed by increasing and then decreasing the activation energy for $\alpha \geq 0.11$; indicating increasing difficulty in the progress of reaction. The second step is probably involving competiting between the reduction of magnetite to iron and sintering process which may account for the increasing dependence of $E$ on $\alpha$.

Fig. 7 exhibits the morphological aspects of the reduction products using SEM studies at the initial and activated samples. Unlike the initial sample, the partial sintering can be clearly observed in the mechanically activated hematite. The partial sintering leads to the formation of rounded particles in the activated sample as a consequence of mass transport process by moving mass from particle surface and internal mass sources [45]. It seems that the agglomeration of the finely ground particles during extended dry milling facilitates the sintering process. The clusters of the partially sintered material can be further observed due to the formation of massive and compact agglomerates which was identified and reported during intensive dry grinding process elsewhere [46].

### 4.3.1. The evaluation of pre-exponential factor

The Coats–Redfern analysis of the thermogravimetric data recorded at a single heating rate has been carried out by inserting various $g(\alpha)$ in Appendix A into Eq. (6) that results in a set of Arrhenius parameters determined from the plot $\ln g(\alpha)/T^2$ versus $1/T$. Similar calculations were made for other heating rates and samples. It was found that each TG curve could be equally well described by several kinetic models resulting in correlation coefficients close to unity. Therefore, the Arrhenius parameters derived were highly variable, exhibiting a strong dependence on the reaction function chosen and a weak dependence on the heating rate. This extra flexibility in the fitting procedure introduces errors in the functional form of the reaction model. This can be offset by making compensation errors in the Arrhenius parameters. Vyazovkin et al. [38,47,48] explored widely artificial isokinetic relationship (IKR) that occurs on fitting various reaction models to the same set of nonisothermal kinetic data. Originally, this procedure was suggested [48] for estimating the pre-exponential factor in the isoconversional method as applied to a single-step process. However, the procedure can be applied to isolate the $\ln A$ on $\alpha$ dependence for multi-step processes [38]. Use of the so-called artificial isokinetic relationship may be used to evaluate the pre-exponential factors for the model-free anal-

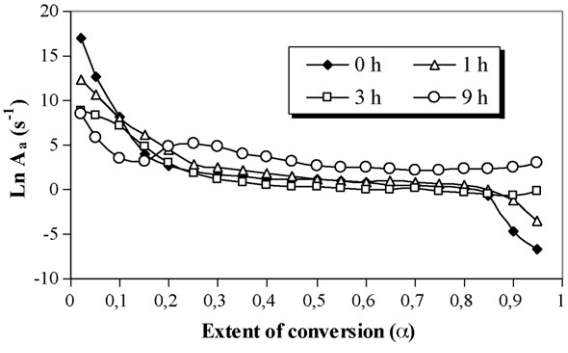


Fig. 9. Dependence of $\ln A_\alpha$ on extent of conversion, $\alpha$, estimated from Eq. (9) for different samples.

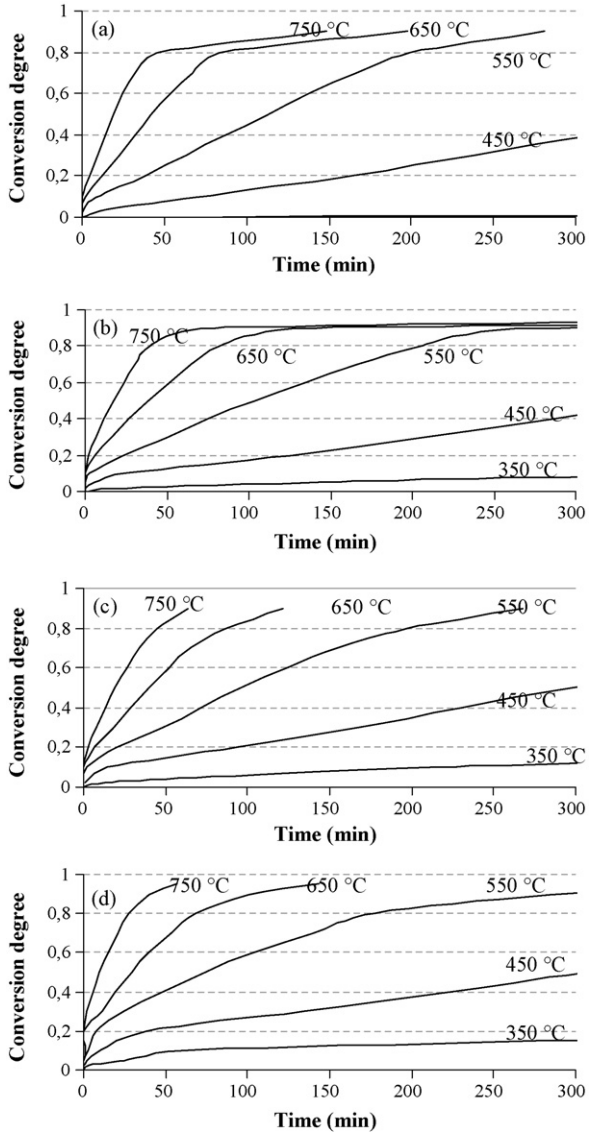


Fig. 10. Prediction at different temperatures using heating rate of 10 °C/min for the initial sample (a) and mechanically activated samples for 1(b), 3 (c) and 9 (d) hours.

ysis. It is observed that the values of the activation energy and pre-exponential factor, obtained for different function of $g(\alpha)$, are correlated through the following relation of compensation:

$$\ln A_i = aE_i + b \quad (9)$$

where the subscript i refers to the one of the possible models considered ($g(\alpha)$ in Appendix A) to describe the process. This reveals that the rate of process can be fairly described by Eq. (6) with practically any model $g(\alpha)$ and fitting $k(T)$ which compensates the error of reaction model choice. An example of artificial isokinetic relationship for the initial sample is given in Fig. 8. All of the plots represent excellent fit where the correlation coefficient exceeds 0.97.

Once the correlation coefficients of the artificial isokinetic relationships have been evaluated, the $E_a$ values from the isoconversional methods are substituted for $E_a$ in the compensation effect Eq. (9) [38] for the studied systems to estimate the corresponding $\ln A_a$ values and obtaining the dependence of $\ln A_a$ on $\alpha$. The results are summarized in Fig. 9. Clearly, the $\ln A_a$ shows the same dependence on $\alpha$ as the apparent activation energies ($E$).

#### 4.3.2. Predictions

Predictions are among the most important practical feature of kinetic analysis [42]. They are widely used to evaluate the kinetic behavior of materials beyond the temperature region of experimental measurements. By using Eq. (8), with nonisothermal kinetic data, the prediction of samples behavior in isothermal conditions is possible. Fig. 10 presents conversion curves of the reduction of the initial sample and ground samples in the mill as a function of time, for different temperatures. On the basis of the curves obtained for the samples, one may state that the conversion time decreases as a function of temperature. It is evident from the graph that the initial sample does not reduce at 350 °C as opposed with mechanically activated hematite. This agrees with our nonisothermal experiments where the onset of reaction for the initial sample is calculated about 420 °C. It follows from the figure that a conversion of 0.1 is attainable for 70, 26, 14 and 10 min at $T = 450$ °C in the initial sample and ground samples for 1, 3 and 9 h, respectively. With increasing temperature, the difference between the samples for achieving a given conversion at an identical temperature reduces. Achieving a conversion of 0.7 at $T = 650$ in the initial sample and activated samples for 1,3 and 9 h, respectively, takes about 67, 65, 65.2 and 58 min that samples are maintained under reducing program. The results reveal that the mechanical activation has large positive effect on the reduction of hematite at lower temperatures compared with reduction at higher temperatures.

## 5. Conclusion

The reduction of $Fe_2O_3$ to Fe was found to occur in a two step process via $Fe_3O_4$. The TG and DTG analysis showed that the two reduction steps took place consecutively. The mechanical activation promoted partial amorphous solids along with some structural distortions in hematite. This pretreatment resulted in improved resolution of overlapping reduction events. The prereduction step in the activated samples initiated and completed at lower temperatures than that in non-activated samples. The activation energy of the first step of reduction decreased with increasing the grinding time. Intensive milling increased slightly the average activation energy of the second reduction step due to the present of finely agglomerated particles and intensive sintering of the particles in higher temperature ranges.

Our study shows that the activation energy of the two steps of the reduction depends greatly on the extent of conversion, implicating that the reduction of hematite to magnetite and magnetite to iron features multi-step characteristics. The decreasing trend of activation energy in the two steps of the reduction can be explained in the terms of a nucleation and growth the

Table A.1
Solid state rate expressions for different reaction models

| Model | Differential form $f(\alpha) = \frac{1}{k}\frac{d\alpha}{dt}$ | Integral form $g(\alpha) = kt$ |
|---|---|---|
| Nucleation models | | |
| Power law (P2) | $2\alpha^{(1/2)}$ | $\alpha^{(1/2)}$ |
| Power law (P3) | $3\alpha^{(2/3)}$ | $\alpha^{(1/3)}$ |
| Avarami-Erofe'ev (A1.5) | $3(1-\alpha)[-\ln(1-\alpha)]^{1/3}/2$ | $[-\ln(1-\alpha)]^{2/3}$ |
| Avarami-Erofe'ev (A2) | $2(1-\alpha)[-\ln(1-\alpha)]^{1/2}$ | $[-\ln(1-\alpha)]^{1/2}$ |
| Avarami-Erofe'ev (A3) | $3(1-\alpha)[-\ln(1-\alpha)]^{2/3}$ | $[-\ln(1-\alpha)]^{1/3}$ |
| Avarami-Erofe'ev (A4) | $4(1-\alpha)[-\ln(1-\alpha)]^{3/4}$ | $[-\ln(1-\alpha)]^{1/4}$ |
| Geometrical contraction models | | |
| Contracting area (R2) | $2(1-\alpha)^{1/2}$ | $[1-(1-\alpha)^{1/2}]$ |
| Contracting volume (R3) | $3(1-\alpha)^{2/3}$ | $[1-(1-\alpha)^{1/3}]$ |
| Diffusion models | | |
| 1D Diffusion (D1) | $1/(2\alpha)$ | $\alpha^2$ |
| 2D Diffusion (D2) | $[-\ln(1-\alpha)]^{-1}$ | $[(1-\alpha)\ln(1-\alpha)]+\alpha$ |
| 3D Diffusion–Jander Eq. (D3) | $(3/2)(1-\alpha)^{2/3}[1-(1-\alpha)^{1/3}]^{-1}$ | $[1-(1-\alpha)^{1/3}]^2$ |
| Ginstling–Brounshtein (D4) | $(3/2)(1-\alpha)^{-1/3}-1)^{-1}$ | $(1-2\alpha/3)-(1-\alpha)^{2/3}$ |
| Reaction-order models | | |
| Zero-order (F0/R1) | 1 | $\alpha$ |
| First-order (F1) | $(1-\alpha)$ | $-\ln(1-\alpha)$ |
| Second-order (F2) | $(1-\alpha)^2$ | $(1-\alpha)^{-1}-1$ |
| Third-order (F3) | $(1-\alpha)^3$ | $0.5[(1-\alpha)^{-2}-1]$ |

model of reduction in which the activation energy required during nucleation is higher than that needed in the growth stage (autocatalytic effects). The prediction of reduction behavior of the samples revealed that with increasing temperature, the difference between the samples for achieving a given conversion reduces at an identical temperature.

## Appendix A

See Table A.1 for solid state rate expressions for different reaction models.

## References


[1] A. Pineau, N. Kanari, I. Gaballah, Thermochim. Acta 447 (2006) 89.
[2] M.V.C. Sastri, R.P. Viswanath, B. Viswanath, Int. J. Hydrogen Energy 7 (1982) 95.
[3] O.J. Wimmers, P. Arnoldy, J.A. Moulijn, J. Phys. Chem. 90 (1986) 1331.
[4] M. Shimokawabe, R. Furuichi, T. Ishii, Thermochim. Acta 28 (1979) 287.
[5] T.L. Joseph, Trans. AIME 120 (1936) 72.
[6] R.J. Fruehan, Y. Li, L. Brabie, E.J. Kim, Scand. J. Metall. 34 (2005) 205.
[7] H.S. Ray, N. Kundu, Thermochim. Acta 101 (1986) 107.
[8] R.P. Viswanath, B. Viswanath, M.V.C. Sastri, React. Kinet. Catal. Lett. 2 (1975) 51.
[9] P. Bálaž, Extractive Metallurgy of Activated Minerals, first ed., Elsevier, Amsterdam, 2000.
[10] H. Hu, Q. Chen, Z. Yin, P. Zhang, Thermochim. Acta 398 (2003) 233.
[11] H. Hu, Q. Chen, Z. Yin, P. Zhang, J. Zou, H. Che, Thermochim. Acta 389 (2002) 79.
[12] H. Hu, Q. Chen, Z. Yin, P. Zhang, L. Ye, Metall. Mater. Trans. 34A (2003) 793.
[13] Q. Chen, H. Hu, Z. Yin, P. Zhang, L. Ye, Metall. Mater. Trans. 33B (2002) 897.
[14] N.J. Welham, Int. J. Miner. Process. 67 (2002) 187.
[15] M. Zdujic, C. Jovalekic, L.J. Karanovic, M. Mitric, D. Poleti, D. Skala, Mater. Sci. Eng. A245 (1998) 109.
[16] T. Kosmac, T.H. Courtney, J. Mater. Res. l7 (1992) 1519.
[17] S. Vyazovkin, Int. Rev. Phys. Chem. 17 (1998) 407.
[18] M.E. Brown, M. Maciejewski, S. Vyazovkin, R. Nomen, J. Sempere, A. Burnham, J. Opfermann, R. Strey, H.L. Anderson, A. Kemmler, R. Keuleers, J. Janssens, H.O. Desseyn, C.R. Li, T.B. Tang, B. Roduit, J. Malek, T. Mitsuhashi, Thermochim. Acta 355 (2000) 125.
[19] A.K. Burnham, Thermochim. Acta 355 (2000) 165.
[20] M. Maciejewski, Thermochim. Acta 355 (2000) 145.
[21] B. Roduit, Thermochim. Acta 355 (2000) 171.
[22] S. Vyazovkin, Thermochim. Acta 355 (2000) 155.
[23] A. Khawam, D.R. Flanagan, Thermochim. Acta 429 (2005) 93.
[24] A. Ortega, Thermochim. Acta 284 (1996) 379.
[25] J.H. Flynn, L.A. Wall, J. Res. Natl. Bur. Stand. Sect. A 70 (1966) 487.
[26] S. Vyazovkin, D. Dollimore, J. Chem. Inf. Comput. Sci. 36 (1996) 42.
[27] T. Ozawa, Bull. Chem. Soc. Jpn. 38 (1965) 1881.
[28] H. Friedman, J. Polym. Sci. C6 (1965) 195.
[29] S. Vyazovkin, N. Sbirrazzuoli, Macromol. Chem. Phys. 200 (1999) 2294.
[30] N. Sbirrazzuoli, Y. Girault, L. Elégant, Thermochim. Acta 293 (1997) 25.
[31] S. Vyazovkin, J. Comput. Chem. 18 (1997) 393.
[32] A.W. Coats, J.P. Redfern, Nature 201 (1964) 68.
[33] A.W. Coats, J.P. Redfern, J. Polym. Sci. B: Polym. Lett. 3 (1965) 917.
[34] H.E. Kissinger, J. Anal. Chem. 29 (1957) 1702.
[35] T. Akahira, T. Sunose, J. Res. Report Chiba Inst. Technol. (Sci. Technol.) 16 (1971) 22.
[36] A. Chakraborty, J. Magn. Magn. Mater. 204 (1999) 57.
[37] S. Vyazovkin, C.A. Wight, Thermochim. Acta 340–341 (1999) 53.
[38] S. Vyazovkin, Int. J. Chem. Kinet. 28 (1996) 95.
[39] G. Munteanu, L. Ilieva, D. Andreeva, Thermochim. Acta 329 (1999) 157.
[41] S. Vyazovkin, C.A. Wight, Annu. Rev. Phys. Chem. 48 (1997) 125.
[40] M.J. Tiernan, P.A. Barnes, G.M.B. Parkes, J. Phys. Chem. 105 (2001) 220–228.
[42] S. Vyazovkin, W. Linert, Int. J. Chem. Kinet. 27 (1995) 73.
[43] S.V. Vyazovkin, A.I. Lesnikovich, V.A. Lyutsko, Thermochim. Acta 165 (1990) 17.
[44] S.V. Vyazovkin, A.I. Lesnikovich, Thermochim. Acta 165 (1990) 273.
[45] R.M. German, Sintering theory and practice, John Wiley and Sons, New York, USA, 1996.
[46] P. Pourghahramani, E. Forssberg, Int. J. Miner. Process. 79 (2006) 120–139.
[47] S. Vyazovkin, W. Linert, Chem. Phys. 193 (1995) 109.
[48] S. Vyazovkin, A.I. Lesnikovich, Thermochim. Acta 128 (1988) 297.